Lasers in Medical Science (2019) 34:525–535
https://doi.org/10.1007/s10103-018-2627-1

ORIGINAL ARTICLE

Biochemical changes in injured sciatic nerve of rats after low-level laser therapy (660 nm and 808 nm) evaluated by Raman spectroscopy

Melissa de Almeida Melo Maciel Mangueira[1] · Nilton Maciel Mangueira[2] · Ozimo Pereira Gama Filho[2] · Márcio Moysés de Oliveira[2] · Renato Albuquerque Heluy[2] · Landulfo Silveira Jr[3] · Egas Caparelli Moniz de Aragão Dáquer[4]

Received: 24 May 2018 / Accepted: 27 August 2018 / Published online: 22 September 2018

Abstract

The aim of this study was to identify biochemical changes in sciatic nerve (SN) after crush injury and low-level laser therapy (LLLT) with 660 nm and 808 nm by Raman spectroscopy (RS) analysis. A number of 32 Wistar rats were used, divided into four groups (control 1, control 2, LASER 660 nm, and LASER 808 nm). All animals underwent surgical procedure of the SN and groups control 2, LASER 660 nm, and LASER 808 nm were submitted to SN crush damage (axonotmesis). The LLLT in the groups LASER 660 nm and LASER 808 nm was applied daily for 21 consecutive days (100 mW, 30 s, 133 J/cm^2 fluence). The hind paw was removed and the SN was dissected and positioned on an aluminum support to collect dispersive Raman spectra (830 nm excitation, 30 s accumulation). To estimate the biochemical changes in the SN associated with LLLT, the principal component analysis (PCA) was applied. The Raman spectra of the sciatic nerve fragments showed peaks of the major biochemical components of the nerve, especially sphingolipids, phospholipids, glycoproteins, and collagen. The spectral features identified in some of the principal component loading vectors are referred to the biochemical elements present on the SN and were increased in the groups treated with LLLT, mainly lipids (sphingo and phospholipids) and proteins (collagen)—constituents of the myelin sheath. The RS was effective in identifying the biochemical differences in the SN after the crush injury, and LASER 660 nm was more efficient than the LASER 808 nm in cell proliferation and repair of the injured SN.

Keywords Peripheral nerve · Low-level laser therapy · Raman spectroscopy · Biochemical changes

Introduction

The peripheral nervous system (PNS) has a great ability to regenerate after a traumatic injury, even in the case of total transection, but functional recovery does not always occur completely [1]. Traumatic injuries by crushing, classified as axonotmesis grade II, despite causing axonal damage with damage of the myelin sheath, maintain the supporting tissue (endoneurium) and are therefore reversible [2, 3]. Such injuries cause neuropathic pain, sensory-motor deficit, and significant morphofunctional impairment [4], and for this reason, this axonotmesis needs to be treated early and properly, since it affects the ability of the nerve impulse to propagate and can cause transient or permanent functional deficits [5–7].

The tissue repair process involves distinct and complex multicellular responses that contribute to reestablishment and reorientation of axons in the injured area. Schwann cells, associated to inflammatory cells and macrophages, express cell

✉ Nilton Maciel Mangueira
nm.mangueira@ufma.br

[1] Department of Physiotherapy, Faculdade Santa Terezinha – CEST, São Luís, Maranhão, Brazil

[2] Department of Morphology, Universidade Federal do Maranhão – UFMA, Cidade Universitária Dom Delgado, Av. dos Portugueses, 1966, Bacanga, São Luís, Maranhão 65080-805, Brazil

[3] Center for Innovation, Technology and Education – CITE, Universidade Anhembi Morumbi – UAM, Parque Tecnológico de São José dos Campos, Estrada Dr. Altino Bondensan, 500, São José dos Campos, São Paulo 12247-016, Brazil

[4] Physiological Sciences Department, Roberto Alcântara Gomes Biology Institute, Rio de Janeiro State University, Avenida Professor Manuel de Abreu, 444/ 5° andar, Vila Isabel, Rio de Janeiro, Rio de Janeiro 20550-170, Brazil

adhesion molecules in the interaction with matrix proteins aiming to remodel the injured area and to promote axonal growth [8], allowing a physical support to the injured area and producing neurotrophic factors, extracellular matrix molecules, and integrins that contribute to the nerve regeneration, besides producing fibronectin, tenascin, heparin sulfate, and collagen to enhance the extracellular matrix lost due to the injury [9].

Early diagnosis of peripheral nerve injury (PNI) is essential in establishing effective therapeutic approaches. Several methods are proposed to identify the PNIs such as magnetic resonance (MR), which evaluates PNI abnormalities by means of changes in signal intensity based on disorganization or loss of nerve fascicular pattern, therefore being a non-invasive technique used for volumetric assessment [10]; electroneuromyography, which diagnoses axonal degeneration through nerve conduction with high sensitivity even in lower degrees of axonal loss [11]; and histomorphometry and immunohistochemistry, the first one is used to measure the repair of nerve tissue through the number of regenerated fibers and the second one is used to identify the distribution and location of specific biomarkers and proteins in different parts of the tissue [12]. Besides the routine use of such techniques, these methods have limitations due to low or no molecular sensitivity, lack of spatial resolution, need for sample preparation, and being time consuming, among others.

Optical techniques such as Raman spectroscopy have been prominent in the biomedical area as a tool for the identification of molecular biomarkers in tissues and fluids aimed at characterization and evaluation of the physiological status in biological processes and diagnoses [13–17]. Compared to immunohistochemical analysis, Raman spectroscopy was effective in the routine chemistry-free diagnosis of peripheral nerve regeneration [13] by examining the biochemical changes of the sciatic nerve after crush injury, showing important peaks in the high wavenumber range (2800 to 3000 cm^{-1}), assigned to phospholipids and proteins. Peaks at 2851, 2885, and 2909 cm^{-1}, which are attributed to phospholipids and CH_2 vibration modes of proteins, reflect the composition of the nerve since the Schwann cells are responsible for the remodeling of the myelin sheath and produce sphingomyelin and proteins. The peak pattern of the axons was distinct from that of the Schwann cells in the same spectral range due to the different composition of both structures [13].

Among the therapeutic resources for PNI, low-level laser therapy (LLLT) is a technique commonly used in clinical practice [18]. Laser has photobiostimulation properties that act directly in pain and functional disability through analgesic and anti-inflammatory effects, muscle relaxation, tissue healing, and fibroblastic proliferation [19, 20]. In the literature, there are many studies that show the effects on the sciatic nerve regeneration process after LLLT [20–22], as well as physiological responses associated to the therapy time [18–22]. However, studies that compare two different wavelengths during 21 days of treatment are hardly found in literature.

The main objective of this work was to identify, by means of Raman spectroscopy, the biochemical changes present in the repair of the sciatic nerve tissue after crush damage and treatment with LLLT irradiation at 660 and 808 nm (133 J/cm^2) during 21 days compared to controls (not injured and injured but not treated). Raman spectroscopy has been used to detect biochemical changes in tendons, knees, and bones as a result of LLLT applied to lesioned tissues with great success [15–17]; therefore, the technique can meet the criteria to detect biochemical changes in injured sciatic nerves by evaluating the differences in the peaks of the irradiated and non-irradiated groups and correlating those peaks with the peaks of the biochemicals present in the tissue.

Materials and methods

Ethical guidelines and samples This experimental study was done in the Maranhão Experimental Surgery Academic League (LACEMA) from Federal University of Maranhão (UFMA) and approved by the Commission of Ethics in the Use of Animals (CEUA) from UFMA, under protocol no. 23115.005396/2016-65. It used 32 female Wistar rats, 7 weeks old, weighing on average 200 g. Animals were randomly divided into four groups of eight animals each (CONTR 1; CONTR 2; LASER 660 nm; LASER 808 nm) and followed for a period of 21 days. All the groups underwent surgical procedure for the exposure of the sciatic nerve (as detailed below). The control 1 group (CONTR 1) did not undergo sciatic nerve damage; in addition to nerve exposure, the other groups (CONTR 2, LASER 660 nm, and LASER 808 nm) were individually submitted to sciatic nerve crush damage, causing axonotmesis. The LLLT was applied only to the groups LASER 660 nm and LASER 808 nm. They were kept in groups of four animals per cage, in a controlled temperature room (23 ± 1 °C) and with 12-h light-dark cycle, receiving proper food and water ad libitum throughout the experimental period of 21 days.

Sciatic nerve injury Each animal was anesthetized with intraperitoneal subcutaneous injection needle (25 × 5 mm), while being held by its back according to the modified protocol of ICB/USP [23]. For the anesthesia, ketamine 10% (90 mg/kg) and xylazine 2% (10 mg/kg) were associated and administered in 0.1 mL/100 g. The anesthesia was confirmed by monitoring the reflex response of tail and cornea, as well as changes of the cardiorespiratory frequencies. Following epilation of the posterior-lateral surface of right thigh, the animal was placed prone on an operating table and antisepsis of the operative

field was done. Under the fenestrated aseptic field, the right sciatic nerve was exposed through skin posterior incision of the lower limb (0.5 cm behind the femur diaphysis and 1 cm above the knee) and divulsion of the posterior muscles of the right paw. The mechanic damage of the sciatic nerve, which causes axonotmesis, was done in the groups CONTR 2, LASER 660 nm, and LASER 808 nm through nerve crush using 16-cm Kelly straight clamp, locked in the second level option, crushing the nerve for 30 s (Fig. 1), which results in a force of approximately 6 N applied to the lesioned nerve [24]. Finally, the wound was sutured and the animal was placed in a cage with water containing analgesics ad libitum.

Low-level laser therapy For the LLLT, it used the TF Premier Plus laser device (MMO Optics, São Carlos, SP, Brazil), consisting of two laser sources: one in the red region (660 nm ± 10 nm of InGalP and 100 mW power) and the other in the infrared region (808 nm ± 10 nm of GaAlAs and 150 mW power). Both lasers were adjusted with the same power (100 mW) to irradiate energy density of 133 J/cm^2 in a beam output area of 0.03 cm^2, being delivered 12 J of total energy (three points of 4 J each) with an exposure time of 30 s. The LLLT was applied daily from the 1st postoperative day, in three points 1 cm apart from each other, perpendicular to the injury surface, with the laser head in contact with the tissue. The control groups received the laser head during the same irradiation time and points with the laser turned off.

On the 21st day of treatment, the rats were anesthetized for surgical removal of the right hind paw together with the right hip and lumbar vertebrae, thus preserving the entire extent of the sciatic nerve. Soon after, the animals were euthanized with overdose of the same anesthetics (ketamine 10% and xylazine 2%), placed in a black bag and discarded in the biological waste. The hind paw was frozen (− 80 °C) and stored during 30 days, being transported with dry ice (− 78 °C) for Raman spectroscopy analysis.

Raman spectroscopy For Raman spectroscopy analysis, the hind paw was unfrozen and the sciatic nerve, which was still inserted in the hind paw, was dissected by removal of the posterior thigh muscles all the way behind the femur, and positioned on an aluminum support (Fig. 2) to be exposed to the excitation laser of the Raman spectrometer. The spectra were obtained by means of a fiber optic probe connected to a dispersive Raman spectrometer, positioned perpendicularly to the nerve.

It used a near-infrared Raman spectrometer (model Dimension P-1, Lambda Solutions, Inc., Waltham, MA, USA) [25–27] with a Raman probe (Vector Probe, Lambda Solutions, Inc., Waltham, MA, USA) for sample excitation and signal collection. This spectrometer has an excitation laser at 830 nm, maximum laser power of 350 mW, imaging spectrograph with diffraction grating coupled to a back thinned, deep-depleted CCD camera (1340 × 100 pixels) of spectral resolution of 2 cm^{-1} in the useful spectral range of 400 to 1800 cm^{-1}. The output laser power was set to 250 mW at the probe tip, thus avoiding sample degradation by heating. The use of a Raman probe allows one to access the Raman spectra of the bulk samples with repeatability in the excitation and collection geometry. The exposure time for collecting the spectra of sciatic nerve was set to 3 s and 10 accumulations, resulting in a shot noise-limited spectrum with an estimated signal-to-noise ratio greater than 50 for the most intense peaks. Spectra were collected in triplicate.

After Raman spectroscopy, the sciatic nerve still inserted in the hind paw was fixed with buffered formalin 10%, and after 24 h, it was sectioned and submitted to standard histology processing.

After collection and storage, spectra were preprocessed in the software Matlab (v. 2007, The Mathworks Inc., Natick, MA, USA), where the background fluorescence was removed by fitting and subtracting a 7th-order polynomial with the "mpoly" routine [26] in the 400–1800 cm^{-1} region. Removal of the fluorescence allows a more appropriate identification of the most relevant peaks without the interference of the broadband fluorescence. Spikes due to cosmic rays were removed manually prior the polynomial subtraction.

Identifying the spectral differences in the groups related to the biochemistry of sciatic nerve Spectra were then submitted to principal component analysis (PCA) in order to reveal the spectral differences between the LLLT-irradiated

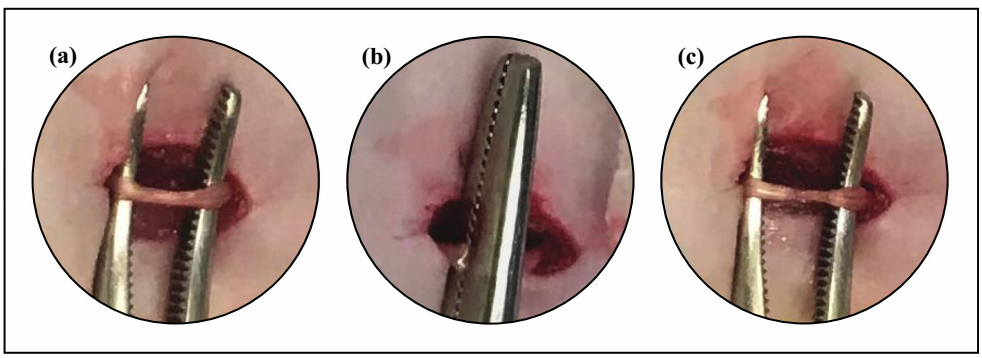

Fig. 1 Surgical process of sciatic nerve injury. (a) shows the dissection and exposure of the sciatic nerve; (b) shows the compression of the nerve with straight Kelly clamp (approximately 6 N force); and (c) shows the exposure of nerve injury after compression

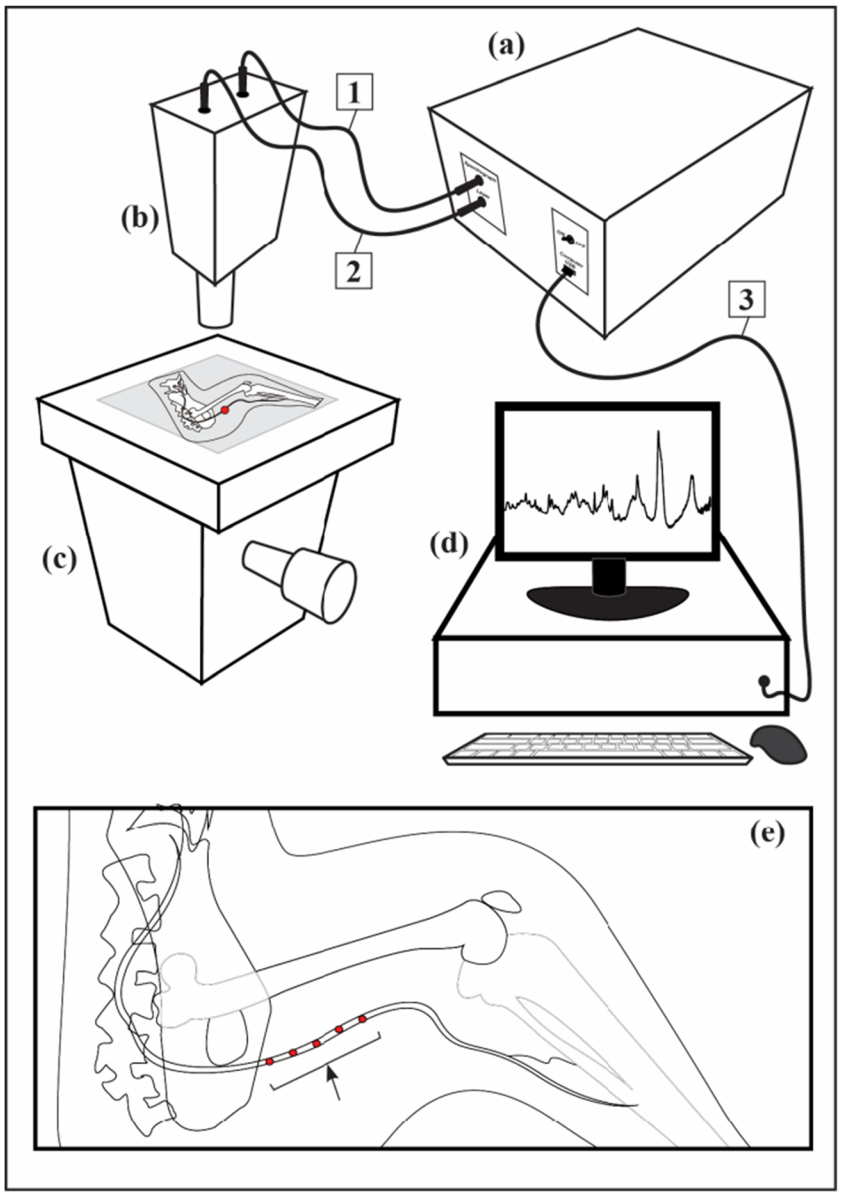

Fig. 2 Schematic diagram of the Raman spectrometer and sample positioned under the probe. The Raman spectrometer (a) connects to the fiber optic Raman probe (b). The laser travels through the excitation fiber (1) and irradiates the sample through the probe (b) held by the aluminum support (c). The scattered signal from the sample is captured (2) and delivered to the spectrograph (a). The electronic-converted spectrum is transferred to the computer (d) by the USB cable port (3). In lateral view, an enlarged illustration of the sample (e) shows the five collection points (arrow) of the Raman spectrum n the sciatic nerve

and LLLT-non-irradiated (control) groups and to correlate these differences with the main biochemicals presented in the sciatic nerve, by comparing the PCA spectral features and the published Raman literature. PCA is a multivariate statistical technique suitable for data reduction and feature extraction that transforms original correlated variables into new uncorrelated variables called principal components loading vectors (LVs), based on the maximum variance and the corresponding scores (SCs) [16, 27]. Each LV is orthogonal to each other, so a unique spectral characteristic is present in each vector. The first LV brings the most relevant spectral features presented in the dataset, and the sequent LVs bring remnant variance vectors, orthogonal with each. The SCs bring the intensity of each LV in each spectrum of the dataset [16, 27].

The parameters LVs and SCs resulting from PCA were used to correlate the changes induced by LLLT in the biochemistry of the sciatic nerve. First, the spectral features of each LV were compared to the biochemical composition of the sciatic nerve in the Raman literature of biological tissues [28–36] and the Raman spectra from a dataset from Silveira et al. [26]. Then, the SCs, which are the intensities of each LV in each spectrum, were associated to differences in the relative concentration of the chemicals associated to the spectral features of that particular LV in each group. The possible differences between the means of the SCs of each experimental group were evaluated by the analysis of variance (one-way or non-parametric ANOVA, when specified) with significance level of 5% ($p < 0.05$), followed by a post-test (Tukey-Kramer or Dunn post hoc test when specified).

Results and discussion

The research was performed over 21 days after the sciatic nerve crush injury to compare the biochemical changes resulting from LLLT at two different wavelengths (660 nm and 808 nm). Figure 3 presents the means Raman spectra of sciatic nerve samples from the four groups evaluated by Raman spectroscopy (control without sciatic nerve injury and without laser treatment—CONTR 1; control with sciatic nerve injury and without laser treatment—CONTR 2; LLLT with red laser—LASER 660 nm; and LLLT with infrared laser 808 nm—LASER 808 nm). The spectra showed Raman peaks in the positions of the main biochemical components of the myelinated peripheral nerve tissue (described in Table 1). By visual inspection, very small spectral differences between the groups were found; therefore, a more detailed exploratory analysis employing multivariate PCA has been performed (Fig. 3).

The peak positions presented in Table 1 were obtained from the first principal component loading vector (Fig. 4, left side). In terms of molecular composition revealed by the Raman bands (Table 1), the main biochemical constituents of the myelin sheath of the sciatic nerve are lipids, especially sphingolipids (718, 1065, and 1440 cm^{-1}) and phospholipids (718, 1085, and 1298 cm^{-1}) [13, 29–33, 37–39]. Raman bands of phospholipids are in similar positions as in glycerol tripalmitate at 877, 1065, 1085, 1130, 1298, and 1440 cm^{-1} [29–34, 39]. Sphingomyelin

Table 1 Peak positions of the main Raman bands of the sciatic nerve spectra shown in the principal component loading vectors (Fig. 4). The band assignments of the main biochemical components responsible for these peaks according to the literature are also presented

Raman shift (cm^{-1})	Band assignment [28–35]
423 (421)*	Cholesterol [31]
(535)*	ν(S–S bridge)—cysteine (proteins, glycoproteins) [32]
546 (545)*	Cholesterol [31]
570	Cholesterol; tryptophan (proteins); cytosine/guanine (nucleic acid) [33]
608	Cholesterol [31, 33]
700 (697)*	ν(C–S)—methionine (proteins); cholesterol [31, 32]
718	C–N (membrane phospholipids head, choline group)—sphingolipids (sphingomyelin) and phospholipids [31, 33]
(766)*	Ring breathing—tryptophan [28]
829 (815, 833)*	Proline, hydroxyproline (collagen), and ring breathing (tyrosine); PO_2^- stretch of nucleic acids—phosphodiester [28, 34, 35]
852 (856, 857)*	Proline, hydroxyproline (collagen) [34]
877 (875)*	C–C–N^+ symmetric stretching (lipids) [35]; antisymmetric stretch vibration of choline group $N^+(CH_3)_3$ (sphingo and phospholipids—phosphatidylcholine) [31]; hydroxyproline (collagen) [28]
(938, 939, 941)*	C–C skeletal—collagen backbone; proline, hydroxyproline (collagen) [33, 34]
1004 (1003, 1006, 1007)*	C–C symmetric ring breathing—phenylalanine (proteins, glycoproteins) [36]
1065 (1062, 1067)*	C–C skeletal stretching and C–O stretching—lipids (sphingo and phospholipids); proline (protein) [28, 31]
1085	C–C skeletal and C–O stretching—unsaturated lipids (sphingo and phospholipids) [31, 33]
1130 (1127, 1132)*	C–N stretching [29] and C–C skeletal acyl backbone—lipids (sphingo and phospholipids) [31, 34]
(1239)*	Amide III (collagen) [32]
1270 (1264)*	C=C groups in unsaturated fatty acids (phospholipids) [31]; amide III (proteins) [28]
1298 (1296, 1301, 1306)*	CH_2 twisting/bending/wagging—unsaturated lipids (sphingo and phospholipids) [31, 32]
(1249)*	C=C stretching (saturated lipids); C–N and N–H modes of amide III (envelope)—proteins [34]
1344	CH_3/CH_2 wagging—proteins/glycoproteins [31]
1440 (1435, 1439)*	CH_3/CH_2 bending modes—lipids (saturated and unsaturated—sphingo and phospholipids); cholesterol [31]
1452	CH_2 bending mode of proteins (collagen) [35]
1469	C=N stretching (proteins) [33]
(1643)*	Amide I—proteins (collagen) [30, 33]
1660 (1658)*	C=C stretching—*cis* in unsaturated fatty acids (sphingo and phospholipids) [31]; C=O stretching (lipids) [35]; amide I (proteins) [30, 33]
(1672)*	Amide I (proteins) [30, 33]
1671 (1658)*	C=O stretching (lipids) [35]; cholesterol [31]

*In parentheses are the peaks found in the principal component loading vectors 2 to 6 that were related to the differences in the constitution of the SN induced by the LLLT

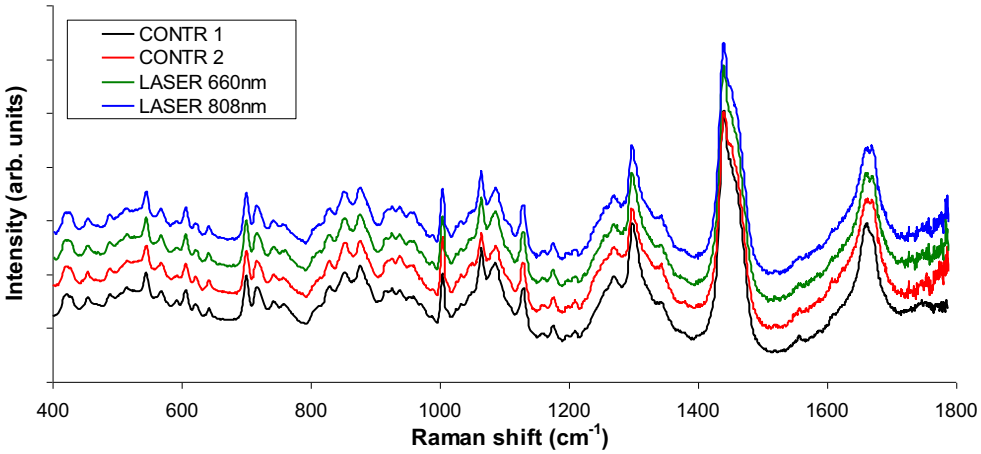

Fig. 3 Mean Raman spectra of the control groups (CONTR 1, no injury; and CONTR 2, injured but not treated) and the groups with LLLT treatment (LASER 660 nm and LASER 808 nm). The spectra are similar, denoting little difference in the constitution. Spectral differences between the groups and the band assignments have been described in the exploratory analysis by PCA

is composed of a ceramide group with an attached phosphatidylcholine residue. Choline bands are located at 718 and 877 cm^{-1} in the Raman spectrum of sphingomyelin [31, 33, 35, 39]. Bands at around 1440 cm^{-1} are typical of fatty acids such as cholesterol band (neutral lipids) as well as CH_2/CH_3 bending modes of saturated and unsaturated fatty acids, and bands due to CC and CH groups for both saturated and unsaturated fatty acids dominate the spectrum in the region from 1000 to 1700 cm^{-1} [29, 31, 33–35].

The myelin sheath also is characterized by peaks of glycoproteins and collagen (535, 852, 941, 1004, 1239, and 1344 cm^{-1}) [32–35]. Approximately 70% of the myelin membrane's dry weight consists of lipids, in particular cholesterol—an important structural lipid element of the myelin membrane—and glycolipids and sulfolipid (highly lipids with long saturated and monosaturated fatty acid chains) [31, 32, 35, 40]. Myelin also contains a specific repertoire of myelin proteins, among which proteolipid protein and myelin basic protein are the most abundant ones [37, 40]. Lipids of the myelin membrane also have phospholipids, cholesterol, plasmalogens, and glycosphingolipids [29, 37, 38]. However, they are not as specific as glycosphingolipids and the sulfated derivative (sulfatide) because of their higher abundance of total lipids [41].

The predominant Raman bands of lipids were assigned to the myelinated peripheral nerve (peaks at 1130, 1298, 1440, and 1660 cm^{-1}), and collagen is found in the surrounding region of peripheral nerves (epineurium) and connective tissue, with bands appearing at 829, 852, 877, 1004, 1239, 1452, and 1660 cm^{-1}. Especially the peaks related to aromatic ring—phenylalanine (1004 cm^{-1}), amide III (1239 cm^{-1}), CH_2 bending (1452 cm^{-1}), and amide I (1660 cm^{-1})—show that these Raman bands are related to type I collagen [30].

To estimate the biochemical changes in the nerve tissue associated with the LLLT in sciatic nerve crush injury, PCA was employed. Multivariate statistics such as PCA can be applied in the Raman spectra to reveal the biochemical constitution of the sample aiming the identification of biochemical changes and diagnosis [16, 26]. The PCA calculates the spectral features of higher variance in the dataset and ranks them according to their importance. With repetition of the experiment, it is possible to identify which bands are important for characterizing the biochemical composition of the tissue in each group (no changes or changes within a particular group) and which ones are introduced in the spectrum as a result of random noise or experimental artifacts [42].

The spectral features presented in the first six LVs (Fig. 4, left) showed Raman bands of main peripheral nerve constituents. The LV 1 showed spectral features of lipids and proteins [31, 39]. Peaks of sphingolipids (particularly sphingomyelin) can be seen at 718, 1065, 1130, 1298, 1440, and 1660 cm^{-1}; peaks of cholesterol can be seen at 423, 546, 570, 608, 700, 1440, and 1671 cm^{-1}; peaks of phospholipids (phosphatidylcholine and phosphatidic acid) can be seen at 718, 1065, 1085, 1298, 1440, and 1660 cm^{-1}; and peaks of proteins (mainly collagen) can be seen at 829, 852, 877, 1004, 1270, 1344, 1452, and 1672 cm^{-1}. The SC 1 (Fig. 4, right) showed that the total amounts of lipids (sphingo and phospholipids) and proteins are different in the groups (ANOVA, $p < 0.001$), being reduced in the CONTR 2 compared to all other groups (Tukey, $p < 0.05$). Since this LV has spectral features of all the gross biochemical constituents of the myelin sheath nerve, and there is no statistically significant difference between the CONTR 1 and the irradiated groups, both light sources acted to recover the gross constitution of the myelin sheath of the sciatic nerve.

The LV 2 showed positive spectral features of proteins at 535, 857, 941, 1004, and 1643–1672 cm^{-1} and negative features of lipids (sphingo and phospholipids) at 1067, 1085, 1301, and 1439 cm^{-1}. The SC 2 showed statistically significant differences between the groups (ANOVA, $p < 0.0001$), being statistically significant the negative intensity of CONTR 1 versus the positive intensity of CONTR 2 (Tukey, $p < 0.001$) and both versus the irradiated groups (Tukey, $p < 0.05$), being the irradiated groups with no significant

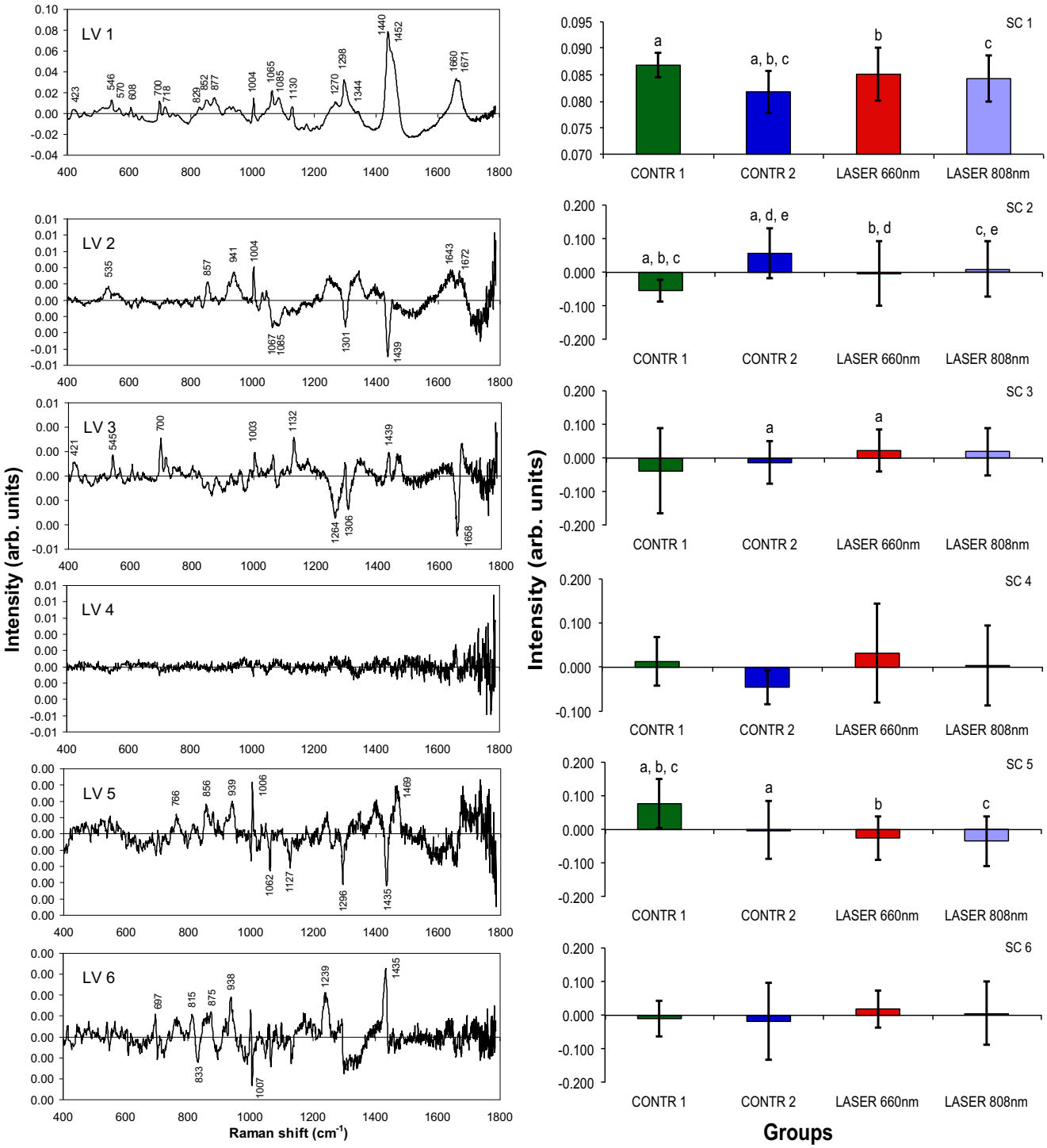

Fig. 4 Left: plot of the first six principal components loading vectors (LV 1 to LV 6) calculated from the Raman spectra. Right: plot of the first six principal component scores (SC 1 to SC 6) and the groups with significance ($p < 0.05$) between the scores of the groups (caption letters). SC 4 was not statistically evaluated. The spectral features observed in the loading vectors relate to the features of biochemical components present in the sciatic nerve (myelin sheath) according to Table 1

differences between them. This shows that the CONTR 1 maintains the lipid constitution (the sphingo and mainly phospholipids) of the preserved myelin sheath, and the CONTR 2 presents proteins (mainly collagen I) characteristic of the injured sciatic nerve. The irradiated groups with "zero" SC 2 suggest that they did not recover the lipids of the myelin sheath nerve as the CONTR 1 group recovered. The LV 3 showed positive peaks referred mainly to cholesterol at 421,

545, 700, and 1439 cm^{-1}, and remnant peaks of proteins at 1003 cm^{-1} and sphingolipids at 1132 cm^{-1}. Negative peaks referred to remnant features of phospholipids are at 1264, 1306, and 1658 cm^{-1}. The SC 3 showed significant differences between the groups (Kruskal Wallis, $p < 0.01$), being the differences occurring for the CONTR 2 and LASER 660 nm (Dunn, $p < 0.05$). In fact, the LASER 660 nm group presented higher SC 3 than all the other groups, and the positive features of the LV 3, related mainly to cholesterol, suggest that the irradiation increased the nervous tissue repair.

The spectral features of the LV 4 are neglectable for the analysis by the lack of peaks referred to lipids and proteins; therefore, the SC 4 has not been statistically evaluated. The LV 5 showed positive peaks at 856, 939, 1006, and 1469 cm^{-1}, attributed to proteins, the peak at 766 cm^{-1} can be assigned to remnant peak from phospholipid, and negative peaks at 1062, 1127, 1296, and 1435 cm^{-1}, attributed to sphingolipids. The SC 5 presented statistical significance between the groups (ANOVA, $p < 0.0001$), and the group CONTR 1 presented significantly higher intensity than the other groups (Tukey, $p < 0.001$), suggesting that the amount of proteins is higher in the non-injured sciatic nerves compared to the injured nerve (maintenance of the protein level expected for the intact nerve compared to the injured groups), and the amounts of lipids are higher for the sciatic nerves irradiated by both light sources. The LV 6 presents general features of proteins and lipids, but the SC 6 showed no significant differences between the groups (ANOVA $< p = 0.269$), indicating no relevant spectral information to describe the biochemical differences between the groups.

In this study, Raman spectroscopy has been used to assay changes in the biochemical composition of sciatic nerve induced by LLLT compared to control. The results showed differences in the peaks referred to lipids (sphingo and phospholipids) and proteins, indicating that these compounds increased with the use of light therapy at 660 and 808 nm, and 4 J/cm^2 compared to the injured control (CONTR 2), thus recovering the myelin sheath of the sciatic nerve to the status of the non-injured sciatic nerve (CONTR 1) (LV 1 and SC 1) after 21 days of treatment. The injured and non-irradiated sciatic nerve presented high proteins as a consequence of the nerve's injury, and the groups that received laser light presented lipid reconstitution (LV 2 and SC 2), suggestive of Schwann cells' proliferative activity induced by both lasers, but significantly higher for the LASER 660 nm due to the presence of high cholesterol content (LV 3 and SC 3). The differences in the protein content in the sciatic nerves can be attributed to collagen, present in the intact sciatic nerve (LV 2 and LV 5, SC 2 and SC 5 respectively) and lower for the injured nerves. Sphingolipids (mainly sphingomyelin), which are the most significant lipids in the nerve's myelin sheath, are remarkably higher in both laser-treated groups compared to the injured and non-treated sciatic nerve group.

Figure 5 shows the binary plots of the SC 1 versus SC 2 and SC 2 versus SC 5 for all the experimental groups, as well as the plot of the ellipses with the 90% confidence interval error for each group. PCA was effective in confirming the molecules present in the sciatic nerve (Fig. 4), where the LV 1 presents the general spectral features of lipids and proteins, LV 2 presenting the spectral features of lipids forms the myelin sheath from intact sciatic nerve and proteins from injured and non-treated nerves, and LV 5 presents spectral features of proteins from intact nerve and lipids from the treated injured nerves. The binary plot of these scores showed a lower scattering of the SCs for both binary plots (SC 1 X SC 2 and SC 2 X SC 5) for the LASER 660 nm and LASER 808 nm, and the ellipses were going towards the CONTR 1 group, principally the ellipse of the LASER 660 nm group. This reveals that both lasers presented effective action in regenerating the myelin sheath in sciatic nerves (more pronounced for the LASER 660 nm), being the constitution closer to the intact nerve in this irradiated group than the injured and untreated CONTR 2. In contrast, the injured CONTR 2 group presented a high dispersion and is dislocated from both laser-irradiated groups.

The LASER 660 nm (red), and in lesser degree the LASER 808 nm (infrared), was efficient in cell proliferation and repair of injured nerve tissue. Both infrared and red lasers have been described as an effective treatment after peripheral nerve injury evaluated by functional and morphometric analyses [21, 22]. When comparing the two wavelengths in LLLT, red laser showed to be more effective than infrared laser to promote early nerve recovery [43], confirming the findings through Raman spectroscopy and PCA analyses. The present study is consistent with the literature, as it provides evidence on the importance of LLLT to improve nerve regeneration through photobiomodulation processes [44]. In this study, LLLT increased the production of lipids (sphingo and phospholipids), glycoproteins, and collagen present in the myelin sheath of sciatic nerve, which is related to tissue repair by stimulating the action and increasing the number of the Schwann cells. In fact, LLLT has shown that the Schwann cell's stimulus contributes to reduce the number of pro-inflammatory cytokines and repairs the neurofilaments and recovers the axonal diameter [19]. Schwann cells take an important role during the nerve regeneration by controlling the influx of the inflammatory cells, cleaning the environment of debris through autophagic process and supporting axonal regrowth [45]. Therefore, Raman spectroscopy is an efficient tool to detect the production of the biochemicals responsible for the sciatic nerve repair (sphingomyelin and collagen) and to measure the efficacy of therapies.

Raman spectroscopy has been described as a relevant technique for the biochemical analysis of biological materials of clinical interest [13–17, 26, 28]. In this research, Raman

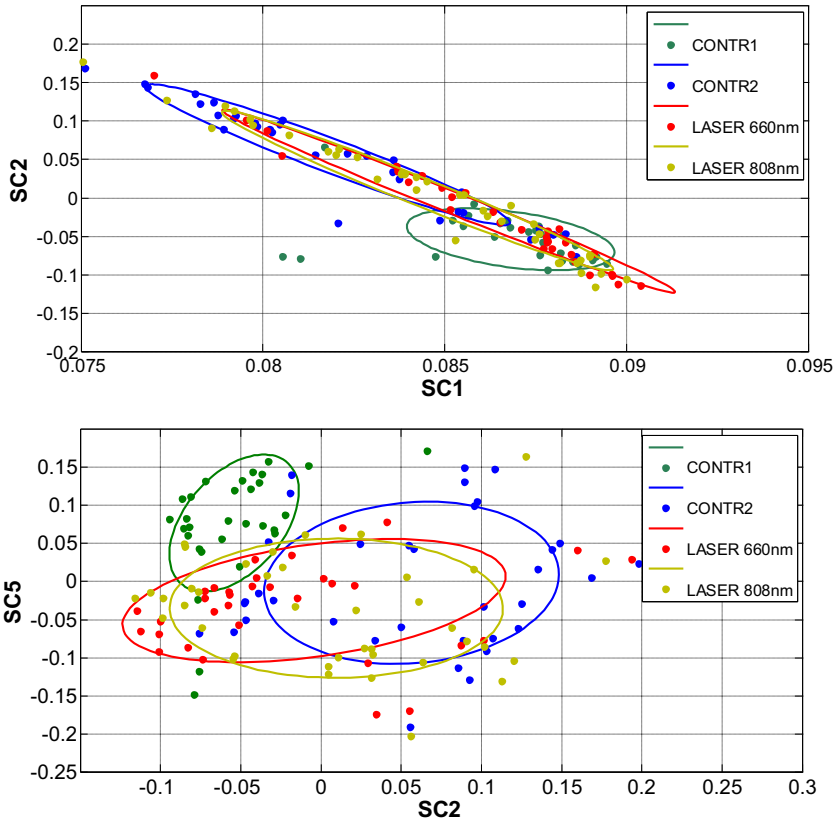

Fig. 5 Binary plot of the principal component scores SC 1 versus SC 2 (top) and SC 2 versus SC 5 (bottom) for each experimental group (CONTR 1, CONTR 2, LASER 660 nm, and LASER 808 nm). The ellipses delimitate the 90% confidence interval error for each group

spectroscopy was effective in the identification and assay of the relative amount of the biochemical components present in the sciatic nerve. The peaks found are directly associated with the chemical composition of the myelin sheath and the Schwann cells (sphingo and phospholipids), both related to the tissue repair of the injured nerve, deposition of glycoproteins (laminin, fibronectin, tenascin, and collagen), and increase of the extracellular matrix in the nerve repair tissue [8, 30].

Conclusion

Raman spectroscopy has been employed to identify the peaks of the major biochemical components of myelinated peripheral nerves (lipids and glycoproteins), and the corresponding biochemical compounds present in the sciatic nerve after crush injury, mainly sphingolipids and phospholipids (attributed to the myelin sheath of the nerve) and collagen (attributed to the epineurium—the external layer of the connective tissue which involves the sciatic nerve). The multivariate analysis by PCA revealed specific differences between the groups, where the spectral characteristics presented in the first six loadings showed Raman bands of the main biochemical constituents of the sciatic nerve. The CONTR 1 group showed Raman spectra characteristic of the biochemical component of the intact nerve, predominance of lipids (sphingo and phospho) and proteins. The loadings LV1, LV2, and LV5, particularly these last two, showed the predominant Raman spectra of sphingo and phospholipids and proteins, mainly in the LASER 660 nm group, and the binary plot between the scores SC1, SC2, and SC5, the ones that presented higher significance between controls and LLLT ($p < 0.05$), showed lower dispersion for the LASER 660 nm group, indicating repair of the sciatic nerve with increased Schwann cells and reconstitution of the myelin sheath after 21 days of LLLT.

Funding information The authors thank FAPEMA (Foundation for Research Support and Scientific and Technological Development of the Maranhão) for the research grant support (Universal Process no. 01377/16), FAPESP (São Paulo Research Foundation) for the partial financial support (Grant no. 2009/01788-5), and CNPq (National Council for Scientific and Technological Development) for the productivity fellowship (Process no. 306344/2017-3). The authors also thank LACEMA (Academic League of Experimental Surgery of Maranhão).

Compliance with ethical standards

Conflict of interest The authors declare that there is no conflict of interest.

Ethical approval It is approved by Commission of Ethics in the Use of Animals (CEUA) from Federal University of Maranhão (protocol no. 23115.005396/2016-65).

References

1. Hoffman PN (2010) A conditioning lesion induces changes in gene expression and axonal transport that enhance regeneration by increasing the intrinsic growth state of axons. Exp Neurol 223(1):11–18. https://doi.org/10.1016/j.expneurol.2009.09.006
2. Seddon HJ (1947) The use of autogenous grafts for the repair of large gaps in peripheral nerves. Br J Surg 35(138):151–167. https://doi.org/10.1002/bjs.18003513808
3. Sunderland S (1951) The function of nerve fibers whose structure has been disorganized. Anat Rec 109(3):503–513. https://doi.org/10.1002/ar.1091090307
4. Ciaramitaro P, Mondelli M, Logullo F, Grimaldi S, Battiston B, Sard A, Scarinzi C, Migliaretti G, Faccani G, Cocito D (2010) Traumatic peripheral nerve injuries: epidemiological findings, neuropathic pain and quality of life in 158 patients. J Peripher Nerv Syst 15(2):120–127. https://doi.org/10.1111/j.1529-8027.2010.00260.x
5. Wu SG, Huang SJ, Zhou J, Sun JY, Guo H, Li FY et al (2014) Dosimetric analysis of the brachial plexus among patients with breast cancer treated with post-mastectomy radiotherapy to the ipsilateral supraclavicular area: report of 3 cases of radiation-induced brachial plexus neuropathy. Radiat Oncol 9(1):1–7. https://doi.org/10.1186/s13014-014-0292-5
6. Brull R, Hadzic A, Reina MA, Barrington MJ (2015) Pathophysiology and etiology of nerve injury following peripheral nerve blockade. Reg Anesth Pain Med 40(5):479–490. https://doi.org/10.1097/AAP.0000000000000125
7. Pereira S, Fontes F, Sonin T, Dias T, Fragoso M, Castro-Lopes JM, Lunet N (2016) Chemotherapy-induced peripheral neuropathy after neoadjuvant or adjuvant treatment of breast cancer: a prospective cohort study. Support Care Cancer 24(4):1571–1581. https://doi.org/10.1007/s00520-015-2935-y
8. Madl CM, Heilshorn SC (2015) Matrix interactions modulate neurotrophinmediated neurite outgrowth and pathfinding. Neural Regen Res 10(4):514–517. https://doi.org/10.4103/1673-5374.155426
9. Elbaz AA, Abu-Almaaty AH, Hassan MK, Mohammed EA, Aziz MM (2017) Therapeutic role of Schwann cells and resveratrol or melatonin combination in peripheral nerve injured rat models. J Exp Appl Anim Sci 2(2):190–210. https://doi.org/10.20454/jeaas.2017.1285
10. Terengui G, Hart A, Wiberg M (2011) The nerve injury and the dying neurons: diagnosis and prevention. J Hand Surg Eur Vol 36(9):730–734. https://doi.org/10.1177/1753193411422202
11. Campbell WW (2008) Evaluation and management of peripheral nerve injury. Clin Neurophysiol 119(9):1951–1965. https://doi.org/10.1016/j.clinph.2008.03.018
12. Geuna S (2015) The sciatic nerve injury model in pre-clinical research. J Neurosci Methods 30(243):39–46. https://doi.org/10.1016/j.jneumeth.2015.01.021
13. Morisaki S, Ota C, Matsuda K, Kaku N, Fujiwara H, Oda R et al (2013) Application of Raman spectroscopy for visualizing biochemical changes during peripheral nerve injury in vitro and in vivo. J Biomed Opt 18(11):116011–116018. https://doi.org/10.1117/1.JBO.18.11.116011
14. Hanlon EB, Manoharan R, Koo TW, Shafer KE, Motz JT, Fitzmaurice M et al (2000) Prospects for in vivo Raman spectroscopy. Phys Med Biol 45(2):R1–R59. https://doi.org/10.1088/0031-9155/45/2/201
15. Moura Júnior MJ, Maia Filho AL, Pessoa DR, Alves MD, Justino Jde S, Andrade Mdos S et al (2015) Assessing the biochemical changes of tendons of rats in an experimental model of tenotomy under therapeutic ultrasound and leds (625 and 945 nm) by near-infrared Raman spectroscopy. Lasers Med Sci 30(6):1729–1738. https://doi.org/10.1007/s10103-015-1779-5
16. Mangueira NM, Xavier M, de Souza RA, Salgado MAC, Silveira L Jr, Villaverde AB (2015) Effect of low-level laser therapy in an experimental model of osteoarthritis in rats evaluated through Raman spectroscopy. J Photomed Laser Surg 33(3):145–153. https://doi.org/10.1089/pho.2014.3744
17. de Souza RA, Xavier M, Mangueira NM, Santos AP, Pinheiro AL, Villaverde AB, LJr S (2014) Raman spectroscopy detection of molecular changes associated with two experimental models of osteoarthritis in rats. Lasers Med Sci 29(2):797–804. https://doi.org/10.1007/s10103-013-1423-1
18. de Oliveira RF, de Andrade Salgado DM, Trevelin LT, Lopes RM, da Cunha SR, Aranha AC et al (2015) Benefits of laser phototherapy on nerve repair. Lasers Med Sci 30(4):1395–1406. https://doi.org/10.1007/s10103-014-1531-6
19. Andreo L, Soldera CB, Ribeiro BG, de Matos PRV, Bussadori SK, Fernandes KPS, Mesquita-Ferrari RA (2017) Effects of photobiomodulation on experimental models of peripheral nerve injury. Lasers Med Sci 32(9):2155–2165. https://doi.org/10.1007/s10103-017-2359-7
20. Andraus RAC, Maia LP, de Souza Lino AD, Fernandes KBP, de Matos Gomes MV et al (2017) LLLT actives MMP-2 and increases muscle mechanical resistance after nerve sciatic rat regeneration. Lasers Med Sci 32(4):771–778. https://doi.org/10.1007/s10103-017-2169-y
21. Takhtfooladi MA, Jahanbakhsh F, Takhtfooladi HA, Yousefi K, Allahverdi A (2015) Effect of low-level laser therapy (685 nm, 3 J/cm^2) on functional recovery of the sciatic nerve in rats following crushing lesion. Lasers Med Sci 30(3):1047–1052. https://doi.org/10.1007/s10103-015-1709-6
22. Ziago EKM, Fazan VPS, Iyomasa MM, Sousa LG, Yamauchi PY, da Silva EA et al (2017) Analysis of the variation in low-level laser energy density on the crushed sciatic nerves of rats: a morphological, quantitative, and morphometric study. Lasers Med Sci 32(2):369–378. https://doi.org/10.1007/s10103-016-2126-1
23. Seabra ID, Pompeu E, Valenti MLG. Anestesia e analgesia de animais utilizados em protocolos experimentais. Central Vivarium of the University of São Paulo Medical School http://www.bioterio.fm.usp.br/pdf/Anestesia_e_Analgesia.pdf. Accessed 08 Mar 2018
24. Handwerker HO, Kobal G (1993) Psychophysiology of experimentally induced pain. Physiol Rev 73(3):639–671. https://doi.org/10.1152/physrev.1993.73.3.639
25. Bispo JA, Vieira EES, Silveira L, Fernandes AB (2013) Correlating the amount of urea, creatinine, and glucose in urine from patients with diabetes mellitus and hypertension with the risk of developing renal lesions by means of Raman spectroscopy and principal component analysis. J Biomed Opt 18(8):87004–870011. https://doi.org/10.1117/1.JBO.18.8.087004
26. Silveira L, Silveira FL, Bodanese B, Zângaro RA, Pacheco MT (2012) Discriminating model for diagnosis of basal cell carcinoma and melanoma in vitro based on the Raman spectra of selected biochemicals. J Biomed Opt 17(7):077003–077015. Erratum in: J Biomed Opt 18(3):039801. https://doi.org/10.1117/1.JBO.17.7.077003
27. Silveira L Jr, Borges RCF, Navarro RS, Giana HE, Zângaro RA, Pacheco MTT, Fernandes AB (2017) Quantifying glucose and lipid components in human serum by Raman spectroscopy and multivariate statistics. Lasers Med Sci 32(4):787–795. https://doi.org/10.1007/s10103-017-2173-2
28. Movasaghi Z, Rehman S, Rehman IU (2007) Raman spectroscopy of biological tissues. Appl Spectrosc 42(5):493–541. https://doi.org/10.1080/05704920701551530
29. Saher G, Stumpf SK (2015) Cholesterol in myelin biogenesis and hypomyelinating disorders. Biochim Biophys Acta 1851(8):1083–1094. https://doi.org/10.1016/j.bbalip.2015.02.010

30. Minamikawa T, Harada Y, Takamatsu T (2015) Ex vivo peripheral nerve detection of rats by spontaneous Raman spectroscopy. Sci Rep 5:17165–17176. https://doi.org/10.1038/srep17165
31. Krafft C, Neudert L, Simat T, Salzer R (2005) Near infrared Raman spectra of human brain lipids. Spectrochim Acta A Mol Biomol Spectrosc 61(7):1529–1535. https://doi.org/10.1016/j.saa.2004.11.017
32. Shetty G, Kedall C, Shepherd N, Stone N, Barr H (2006) Raman spectroscopy: evaluation of biochemical changes in carcinogenesis of oesophagus. Br J Cancer 94(10):1460–1464. https://doi.org/10.1038/sj.bjc.6603102
33. Stone N, Kendall C, Smith J, Crow P, Barr H (2004) Raman spectroscopy for identification of epithelial cancers. Faraday Discuss 126:141–157. https://doi.org/10.1039/B304992B
34. Cheng WT, Liu MT, Liu HN, Lin SY (2005) Micro-Raman spectroscopy used to identify and grade human skin pilomatrixoma. Microsc Res Tech 68(2):75–84. https://doi.org/10.1002/jemt.20229
35. Notingher I, Green C, Dyer C (2004) Discrimination between ricin and sulphur mustard toxicity in vitro using Raman spectroscopy. J R Soc Interface 1(1):79–90. https://doi.org/10.1098/rsif.2004.0008
36. Kateinen E, Elomaa M, Laakkonen UM, Sippola E, Niemela P, Suhonen J, Jarninen K (2007) Quatification of the amphetamine content in seized street samples by Raman spectroscopy. J Forensic Sci 52(1):88–92. https://doi.org/10.1111/j.1556-4029.2006.00306.x
37. Baron W, Hoekstra D (2010) On the biogenesis of myelin membranes: sorting, trafficking and cell polarity. FEBS Lett 584(9):1760–1770. https://doi.org/10.1016/j.febslet.2009.10.085
38. Schmitt S, Castelvetri LC, Simons M (2015) Metabolism and functions of lipids in myelin. Biochim Biophys Acta 1851(8):999–1005. https://doi.org/10.1016/j.bbalip.2014.12.016
39. Fahy E, Subramaniam S, Brown HA, Glass CK, Merrill AH Jr, Murphy RC et al (2005) A comprehensive classification system for lipids. J Lipid Res 46(5):839–861. https://doi.org/10.1194/jlr.E400004-JLR200
40. Zöller I, Meixner M, Hartmann D, Büssow H, Meyer R, Gieselmann V, Eckhardt M (2008) Absence of 2-hydroxylated sphingolipids is compatible with normal neural development but causes late-onset axon and myelin sheath degeneration. J Neurosci 28(39):9741–9754. https://doi.org/10.1523/JNEUROSCI.0458-08.2008
41. Lahiri S, Futerman AH (2007) The metabolism and function of sphingolipids and glycosphingolipids. Cell Mol Life Sci 64(17):2270–2284. https://doi.org/10.1007/s00018-007-7076-0
42. Aguiar RP, Silveira L Jr, Falcão ET, Pacheco MT, Zângaro RA, Pasqualucci CA (2013) Discriminating neoplastic and normal brain tissues in vitro through Raman spectroscopy: a principal components analysis classification model. Photomed Laser Surg 31(12):595–604. https://doi.org/10.1089/pho.2012.3460
43. Barbosa RI, Marcolino AM, de Jesus GRR, Barbieri CH, de Cássia RFM (2010) Comparative effects of wavelengths of low-power laser in regeneration of sciatic nerve in rats following crushing lesion. Lasers Med Sci 25(3):423–430. https://doi.org/10.1007/s10103-009-0750-8
44. de Andrade ALM, Bossini PS, de Souza ALMC, Sanchez AD, Parizotto NA (2017) Effect of photobiomodulation therapy (808 nm) in the control of neuropathic pain in mice. Lasers Med Sci 32(4):865–872. https://doi.org/10.1007/s10103-017-2186-x
45. Cattin AL, Lloyd AC (2016) The multicellular complexity of peripheral nerve regeneration. Curr Opin Neurobiol 39:38–46. https://doi.org/10.1016/j.conb.2016.04.005